Skin Models for Perspiration Simulation

Subjects: Dermatology

Contributor: Jasmina Casals-Terré

Skin models offer an in vitro alternative to human trials without their high costs, variability, and ethical issues. Perspiration models, in particular, have gained relevance lately due to the rise of sweat analysis and wearable technology.

Keywords: skin models ; skin phantom

1. Introduction

The skin is our first interface with the surrounding environment, simultaneously acting as a protective barrier and a sensing platform. Skin studies are necessary to assess its real nature despite the limitations that experimentation on living tissue present. Researchers have been using non-invasive methods for the past decades, with the use of skin replica methods being a well-known example for the study of surface microtopography [1]. In recent years, there has been an increase in the implementation of in vitro models at multiple levels. This way, ethical issues and the high variability of human tests are avoided, while speeding up the testing process thanks to their longer storage stability and lower costs [2]. We have divided the skin models found in the literature into four main groups, depending on their purpose: physical phantoms, skin substitutes, skin-on-a-chip, and perspiration models (Figure 1).

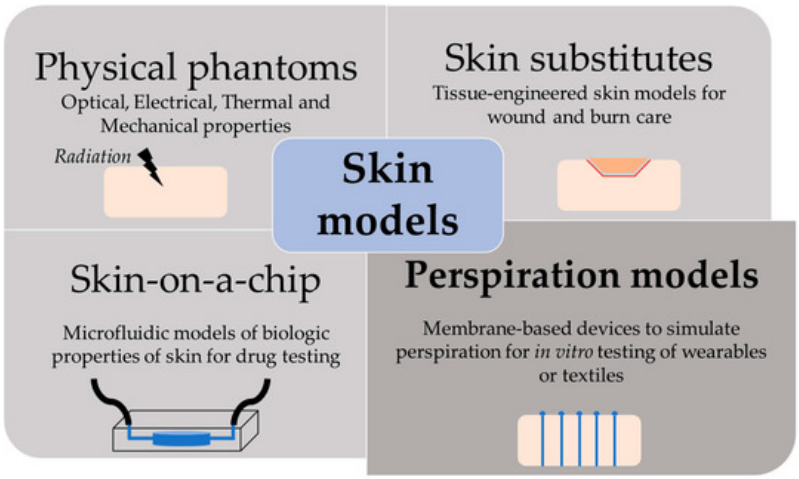

Figure 1. Scheme of the different purpose and applications of skin models.

2. Perspiration Models

The perspiration simulation works found in the literature model the sweat gland as a fluid conduit, discarding to replicate their role on sweat generation. Sweat generation, which takes place in the secretory coil, is replaced by pumping mechanisms, such as syringe pumps and hydrostatic pressure. Although syringe pumps allow for directly setting a specific flow rate and are easier to use, hydrostatic control is sometimes preferred due to its more stable response. Therefore, the models presented are focused on the transport of sweat from a fluid source to a skin-like surface.

Most works use laser systems, specifically, CO_2 lasers, to machine the holes that will simulate sweat gland ductal conduits. CO_2 lasers have been extensively used in rapid manufacturing due to their high versatility and cost-effective operation and maintenance [3]. Their infrared radiation (wavelength range of 9–12 µm) is capable of removing material by thermal ablation. The features' characteristics (width, depth, and geometry) can be tuned by controlling laser parameters, such as the power, speed, and focal distance. These benefits have made CO_2 lasers a well-known tool in microfluidics laboratories for rapid prototyping, without the need for molds or complex equipment [4]. In particular, they are adequately suited for fabricating passing holes in a polymeric substrate, which is the case of the perspiration models listed.

2.1. Laser-Machined Membranes

The first work dedicated to developing a perspiration model was presented by Hou et al. [5] in 2013 (Figure 1a). The authors developed a bi-layer membrane where the bottom membrane (a commercial polycarbonate track-etched membrane) mimics the flow rate of the sweat gland while the top layer provides the proper pore density and surface texture. The bottom membrane must be hydrophilic and with pores small enough to dominate the pressure drop across the system. The top membrane is made of a combination of dry-film photoresists and a polyester substrate. Sweat glands were patterned on the top membrane by CO_2 laser, obtaining a pore diameter of 80 microns with a pore density of 200 pores/cm^2. Skin texture was replicated using a replica resin, achieving a faithful representation of skin texture, while wettability was compromised as the measured contact angle of the membrane differs from the one in human skin. The resulting thin membrane, with a thickness below 100 microns, was integrated into an acrylic holder, and sweat was pumped hydrostatically. The authors validated the sweat rate obtained experimentally using a flowmeter, showing a reasonable agreement with theoretical predictions. In addition, uniform activation of pores across the surface was demonstrated by visual inspection.

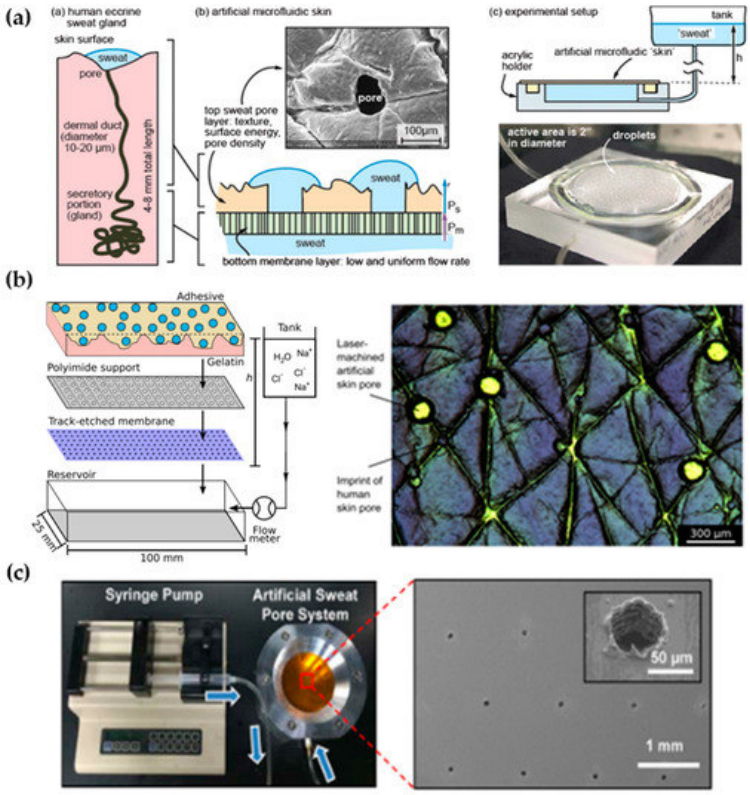

Figure 1. Perspiration models in literature. (a) Schematic of the bi-layer membrane design and its comparison with the sweat gland structure (left). Depiction of the experimental set-up and image of the integrated membrane (right). Reprinted with permission from [5]. Copyright 2013, Royal Society of Chemistry. (b) Scheme showing the layers of the perspiration model by Hansen et al. [6] (left). Adapted with permission from [6]. Copyright 2020, American Chemical Society. Microscopy image of the surface of the artificial skin by Eiler et al. [7] (right). Adapted with permission from [7]. Copyright 2020, Elsevier. (c) Experimental set-up of the artificial sweat pore system used by Koh et al. [6] and SEM image of the perforated membrane. Reprinted with permission from [6]. Copyright 2016, The American Association for the Advancement of Science.

The Thormann group recently adapted a similar membrane for skin adhesive testing [6][7] (Figure 1b). They obtained similar values of pore diameter and water contact angle as they used the same methodology, also reporting roughness measurements with a mechanical profilometer (obtaining an average roughness, R_a, around 10 microns, which is on the same order of magnitude as human skin) and rheology tests. While Eiler et al. [6] used a syringe pump to set the desired sweat rate, Hansen et al. [7] used hydrostatic pumping in combination with a flowmeter. Membrane materials and fabrication steps did not differ greatly from the original work. The only variation was found in Hansen et al. [7], where the outermost layer of the membrane was replaced by a cross-linked gelatin, which hydrates during perspiration better mimics the human stratum corneum. This material modification increased the pore diameter from 87 to 250 μm due to the low compatibility of gelatin with laser processing.

Similarly, Koh et al. [8] developed a perspiration model using pores patterned by laser on a polyimide membrane as part of their experimental set-up (Figure 1c). In this case, a single-layer membrane was used, but as their device was attached completely covering the perspiration zone, the effect of non-uniform pore activation was limited. The membrane was integrated into an aluminum chamber that served as a fluid source and it was controlled by a syringe pump, which was set at a constant flow rate of 5.5 µL/h for a harvesting surface area of 0.07 cm^2.

Liu et al. [9] proposed a fabrication method to overcome the resolution limitation of laser-patterned membranes. The authors developed a skin phantom intended to replicate physical properties, and they included sweat ducts for a closer electrical simulation. They used gelatin to replicate the epidermis, and SU-8 photoresist for the stratum corneum. Using microfabrication techniques (lift-off), the authors fabricated a copper mask with holes mimicking sweat duct diameter on top of the structure before laser ablation. With this method, they reduced the diameter down to the 20 microns of sweat duct, but pore depth remained small in comparison to the values of sweat duct length. In fact, they studied the relation of laser parameters (duration and power of ablation) with the resulting pore depth, estimating a pore depth of hundreds of micrometers for their experimental conditions (ablation time of 0.1 s and laser power of 25 W/mm^2). However, they achieved an average pore depth of under 60 µm. They did not integrate the skin phantom to any fluidic connection as they were interested in its mechanical and electrical properties. In Table 1, there is a summary of the characteristics of these types of perspiration models and their comparison with the reference values of human skin.

Table 1. Comparison of the key parameters of laser-machined perspiration models found in the literature with respect to human skin values.

Work	Sweat Gland Diameter (µm)	Sweat Gland Length (mm)	Sweat Gland Density (cm^{-2})	Contact Angle (°)	Roughness R_a (µm)	Sweat Rate (µL/min·cm^2)	Fabrication Method	Flow Control
Human skin [10]	***10–20***	***1–4***	***100–550***	***80–110*** [11]	***10–50 (RMS)*** [12]	***0.2–4***	-	-
Hou et al. [5]	**80**	**<0.1**	**200**	**θ_a= 76**	-	**0.8–5**	**CO_2 laser**	**Hydrostatic pressure**
Eiler et al. [6]	**86.8 ± 17.5**	**<0.1**	**100**	**69.2 ± 3.6**	**12.1 ± 1.3**	**0.5–2**	**CO_2 laser**	**Syringe pump**
Hansen et al. [7]	**250**	**<0.1**	**100**	**77.5 ± 0.8**	**8.4 ± 4.5**	**0.5–2**	**CO_2 laser**	**Hydrostatic pressure**
Koh et al. [8]	**60**	**<0.1**	**100**	-	-	**1.3**	**CO_2 laser**	**Syringe pump**
Liu et al. [9]	**20 ± 3**	**<0.1**	**620**	-	-	-	**Lift-off + CO_2 laser**	-

2.2. Alternative Approaches

Recent proposals of perspiration models are not reduced solely to laser-machined membranes. With a methodology similar to thermal manikins, Brueck et al. [13] designed an arm mold with casted silicone, which was coupled with a complex electronic system capable to control the desired sweat rate dispensed by a peristaltic pump (from 1 to 500 µL/min) and the salt concentration of the emerging sweat (from 10 to 200 mM) (Figure 2a). Details on the fabrication of the sweat pores are not given in the publication, probably opting for a system of pipes and holes similar to the one used in thermal manikins. Characterization of the flow rates achievable is validated experimentally by gravimetry.

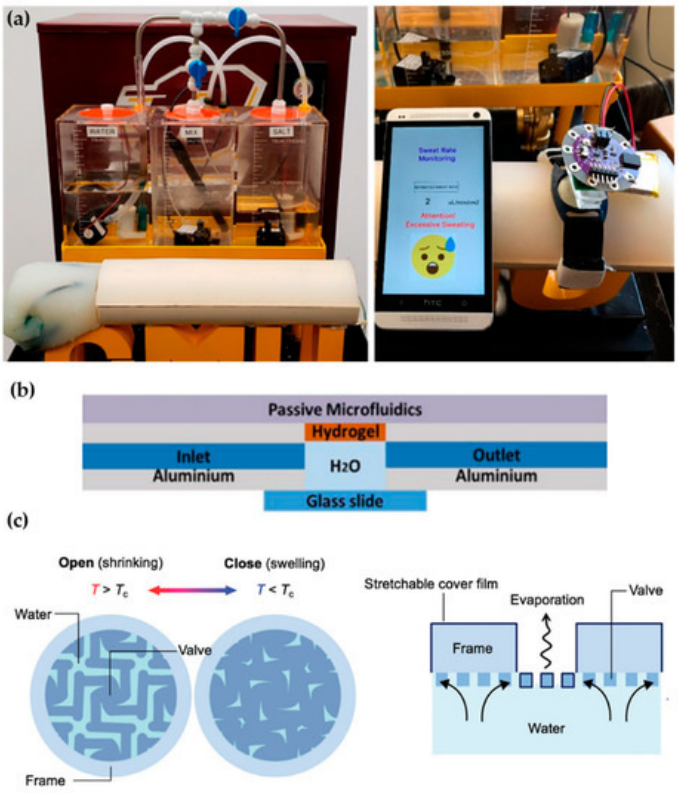

Figure 2. Alternative approaches for perspiration models. (**a**) Image of the sweating arm prototype developed by Brueck et al. [13] showing the arm mold and the fluid tanks for sweat solution (left). In vitro test with a wearable device that monitors sweat rate (right). Adapted with permission from [13]. Copyright 2019, MDPI. (**b**) Schematic cross-section of the artificial skin used by Garcia-Cordero et al. [14]. Adapted with permission from [14]. Copyright 2018, IEEE. (**c**) Schematic of the artificial perspiration membrane for heat dissipation developed by Kim et al. [15]. Adapted with permission from [15]. Copyright 2020, John Wiley and Sons.

Alternative fabrication methods have also been used for sweat gland fabrication such as the additive manufacturing by 3D printing proposed by Turcin et al. [16]. The authors fabricated a shell of a torso by fused deposition modelling (FDM) to integrate a sweating device manufactured by stereolithography (SLA). SLA, where the polymerization of a resin takes place by ultraviolet radiation, was chosen for its good surface finish of the products and resolution. Although it has been shown that SLA can arrive at the dimensions required for the sweat gland [17], the sweating device has a minimum diameter of 0.55 mm, which is much larger than the actual sweat gland diameter. This structure could be adopted as an alternative way to distribute sweat generation in a thermal manikin, but its application in sweat wearable testing would be limited.

Hydrogels offer the possibility to recreate sweating directly through their micrometric porous structure. Garcia-Cordero et al. [14] used an agarose hydrogel as a skin-like fluidic interface to their microfluidic wearable device (Figure 2b). The hydrogel was integrated into an aluminum chamber where sweat was pumped, and it diffused through the hydrogel. Although hydrogels are a good substitute for a soft tissue such as the skin, their intricate three-dimensional pore structure does not correspond with the sweat gland structure.

Kim et al. [15] also used a hydrogel to fabricate an artificial perspiration membrane. However, their aim was to create a refrigeration system inspired in the sweating mechanism. The thermoresponsive hydrogel used served as a valve to regulate evaporation rate at the interface depending on temperature (Figure 2c). When the temperature is higher than the critical temperature (T_c), the hydrogel shrinks, producing an enlargement in the evaporation area. This way, the evaporation and cooling effect can be regulated as a function of the temperature. This example further illustrates the wide variety of characteristics and purposes of skin models.

References

1. Frosch, P.J.; Kligman, A.M. Noninvasive Methods for the Quantification of Skin Functions: An Update on Methodology and Clinical Applications; Springer: Berlin, Germany, 2012.
2. Dąbrowska, A.K.; Rotaru, G.-M.; Derler, S.; Spano, F.; Camenzind, M.; Annaheim, S.; Stämpfli, R.; Schmid, M.; Rossi, R.M. Materials used to simulate physical properties of human skin. Ski. Res. Technol. 2015, 22, 3–14.

3. Snakenborg, D.; Klank, H.; Kutter, J.P. Microstructure fabrication with a CO2 laser system. J. Micromech. Microengin. 2003, 14, 182–189.
4. Matellan, C.; Hernández, A.E.D.R. Cost-effective rapid prototyping and assembly of poly(methyl methacrylate) microfluidic devices. Sci. Rep. 2018, 8, 1–13.
5. Hou, L.; Hagen, J.; Wang, X.; Papautsky, I.; Naik, R.; Kelley-Loughnane, N.; Heikenfeld, J. Artificial microfluidic skin for in vitro perspiration simulation and testing. Lab Chip 2013, 13, 1868–1875.
6. Eiler, J.; Hansen, D.; Bingöl, B.; Hansen, K.; Heikenfeld, J.; Thormann, E. In vitro evaluation of skin adhesives during perspiration. Int. J. Adhes. Adhes. 2020, 99, 102574.
7. Hansen, D.; Moghaddam, S.Z.; Eiler, J.; Hansen, K.; Thormann, E. Performance of Polymeric Skin Adhesives during Perspiration. ACS Appl. Polym. Mater. 2020, 2, 1535–1542.
8. Koh, A.; Kang, D.; Xue, Y.; Lee, S.; Pielak, R.M.; Kim, J.; Hwang, T.; Min, S.; Banks, A.; Bastien, P.; et al. A soft, wearable microfluidic device for the capture, storage, and colorimetric sensing of sweat. Sci. Transl. Med. 2016, 8, 366ra165.
9. Liu, C.; Huang, Y.; Li, S.; Chen, Y.; Wang, W.Z.; Yu, J.; Shih, W. Microelectromechanical system-based biocompatible artificial skin phantoms. Micro Nano Lett. 2019, 14, 333–338.
10. Sonner, Z.; Wilder, E.M.; Heikenfeld, J.; Kasting, G.B.; Beyette, F.R.; Swaile, D.; Sherman, F.F.; Joyce, J.L.; Hagen, J.A.; Kelleyloughnane, N.; et al. The microfluidics of the eccrine sweat gland, including biomarker partitioning, transport, and biosensing implications. Biomicrofluidics 2015, 9, 031301.
11. Kovalev, A.E.; Dening, K.; Persson, B.N.J.; Gorb, S.N. Surface topography and contact mechanics of dry and wet human skin. Beilstein J. Nanotechnol. 2014, 5, 1341–1348.
12. Qu, M.; Hamdani, S.; Bunce, J.A. The physiology and genetics of stomatal adjustment under fluctuating and stressed environments. In Applied Photosynthesis: New Progress; Intech: London, UK, 2016.
13. Brueck, A.; Bates, K.; Wood, T.; House, W.; Martinez, Z.; Peters, S.; Root, B.; Yelamarthi, K.; Kaya, T. An Artificial Sweating System for Sweat Sensor Testing Applications. Electronics 2019, 8, 606.
14. Garcia-Cordero, E.; Wildhaber, F.; Bellando, F.; Longo, J.; Fernandez-Bolanos, M.; Guerin, H.; Ionescu, A.M. Embedded passive nano-liter micropump for sweat collection and analysis. In Proceedings of the 2018 IEEE Micro Electro Mechanical Systems (MEMS), Belfast, Northern Ireland, 21–25 January 2018; pp. 1217–1220.
15. Kim, J.; Im, S.; Kim, J.H.; Kim, S.M.; Lee, S.M.; Lee, J.; Im, J.P.; Woo, J.; Moon, S.E. Artificial Perspiration Membrane by Programmed Deformation of Thermoresponsive Hydrogels. Adv. Mater. 2020, 32, 1–7.
16. Turcin, I.; Cosma, C.; Abdallah, A.; Balc, N. Design for Additive Manufacturing a Sweat Gland Simulator. In Proceedings of the 7th International Conference on Additive Technologies, Maribor, Slovenia, 10–11 October 2018.
17. Gong, H.; Bickham, B.P.; Woolley, A.T.; Nordin, G.P. Custom 3D printer and resin for 18 μm × 20 μm microfluidic flow channels. Lab Chip 2017, 17, 2899–2909.